High-order accurate Cartesian partitioning methods. Application to rotor flows

O. Saunier, S. Peron, G. Jeanfaivre, C. Benoit[1] , A. Lerat[2]

[1]CFD and Aeroacoustics Departement, ONERA
29, Avenue de la Division Leclerc, BP 72, 92322 Chatillon Cedex, France
olivier.saunier@onera.fr, stephanie.peron@onera.fr, gaelle.jeanfaivre@onera.fr, christophe.benoit@onera.fr

[2]SINUMEF Laboratory, ENSAM, 151 bd de l'Hôpital, 75013 Paris, France
alain.lerat@paris.ensam.fr

Key words: Mesh adaptation method, high-order schemes, chimera method

Abstract. In the present article, a coupling between the mesh adaptation technique of Meakin and high-order numerical schemes is proposed. Several schemes for introducing an artificial dissipation into a high-order central finite volume approximation to the Euler equations are considered. Transfers in overlap regions are completed by high-order interpolations. The method is applied to the computation of 2D parallel blade-vortex interaction and to the simulation of a 3D flow around a hovering blade of the ONERA 7A helicopter rotor exhibiting an improvement in the wake capture.

1 Introduction

Accurate numerical computation of helicopter rotor flows requires very fine meshes to capture accurately the blade tip vortex. As a matter of fact, previous computations of rotorcraft flows[14,15] demonstrated that the tip vortex is strongly diffused during the first passage even in computations performed with 10 million grid points. These computations have been realized on curvilinear structured meshes and suffered from an non adapted distributoin of the grid points and unsufficient density of the mesh to capture the tip vortex. In order to reduce the numerical diffusion, mesh adaptive methods are considered for the calculation of vortical flows since the scales in the flow variables differ greatly throughout the computational domain. The use of mesh adaptation techniques significantly reduces the involved computational time and memory. During last years, previous works in the litterature on grid adaptation methods are numerous and it would be impossible to report all of them. Generally speaking, there is a wealth of publication concerning unstructured meshes adaptation technique in finite element formulation. On the other hand, there is a paucity of work for structured meshes in finite volume and finite difference approaches. Meakin[10] proposed a mesh adaptive method within systems of overset Cartesian grids. This technique, based on Chimera method, has been also developed by Benoit and Jeanfaivre[1] and applied with a second-order scheme to the capture of the vortical wake of helicopter rotors in hovering flight.

On the other hand, computations realized with high-order accurate schemes[4, 12, 16] proved that significant improvements in the accuracy of rotor performance predictions can be obtained with just a small increase in computing cost. The objective of this paper is to improve the mesh adaptation technique of Meakin by increasing the accuracy order of numerical scheme.
First, we present the high-order numerical schemes on curvilinear and Cartesian meshes and we describe the new developments in Chimera method. The capabilites of the high-order method in computing accurately vortex flow is assessed by inviscid simulations of 2D parallel blade-vortex interaction and of a 3D flow around a hovering blade of helicopter rotor.

2 High-order numerical schemes

2.1 Third-order finite volume scheme on curvilinear meshes

On curvilinear grids, a third-order space accurate scheme is used. This scheme is based on the work is of Cinnella, Lerat and Rezgui[3, 13] in a finite-volume formulation. For the sake of simplicity, this scheme is presented in 2D. Let p, ρ, u, v, E and H denote the pressure, density, Cartesian velocity components, total energy and total enthalpy. For a perfect gas:

$$p = (\gamma - 1)\rho\Big(E - \frac{u^2 + v^2}{2}\Big)$$

where γ is the ratio of specific heats. The Euler equations for two dimensional inviscid flow can be written in integral form:

$$\frac{d}{dt}\int_{\Omega} w \, d\Omega + \int_{\partial\Omega} F(w).n \, d\Gamma = 0, \tag{1}$$

where:

$$w = \begin{pmatrix} \rho \\ \rho u \\ \rho v \\ \rho E \end{pmatrix}, \qquad f(w) = \begin{pmatrix} \rho u \\ \rho u^2 + p \\ \rho uv \\ \rho u H \end{pmatrix}, \qquad g(w) = \begin{pmatrix} \rho v \\ \rho uv \\ \rho v^2 + p \\ \rho v H \end{pmatrix}$$

and Ω is a bounded domain with boundary $\partial\Omega$, n is the unit outward normal to $\partial\Omega$, and $F(w) = [f(w), g(w)]$ is the flux density. We define a structured mesh composed of quadrangular cells $\Omega_{j,k}$ (see Figure 1) and denote the cell centers by $C_{j,k}$, and the cell edges by $\Gamma_{j+\frac{1}{2},k}$ or $\Gamma_{j,k+\frac{1}{2}}$:

$$\partial\Omega_{j,k} = \{\Gamma_{j+\frac{1}{2},k},\ \Gamma_{j,k+\frac{1}{2}},\ \Gamma_{j-\frac{1}{2},k},\ \Gamma_{j,k-\frac{1}{2}}\}$$

Applied to the cell $\Omega_{j,k}$, the conservation laws (1) become:

$$\frac{d}{dt}\int_{\Omega_{j,k}} w \, d\Omega + \sum_{\Gamma \in \partial\Omega_{j,k}} \int_{\Gamma} F(w).n \, d\Gamma = 0,$$

The numerical flux density $F_{j+\frac{1}{2},k}$ through the edge $\Gamma_{j+\frac{1}{2},k}$ of the cell $\Omega_{j,k}$, is an approximation to:

$$\frac{1}{|\Gamma_{j+\frac{1}{2},k}|}\int_{\Gamma_{j+\frac{1}{2},k}} F(w).n \; d\Gamma$$

To define a local reference frame on the edge $\Gamma_{j+\frac{1}{2},k}$, let ξ be an axis passing through the adjoining cell center, oriented from $C_{j,k}$ to $C_{j+1,k}$ and let η be an axis on $\Gamma_{j+\frac{1}{2},k}$. Let E be the intersection point of the η and ξ axis. Performing a Taylor expansion in the

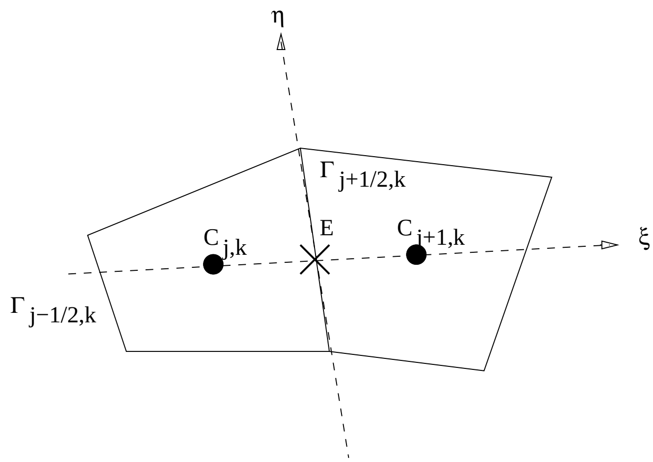

Figure 1: *Definition of the local frame of reference*

η-direction, a third-order approximation of the exact flux is:

$$\frac{1}{|\Gamma_{j+\frac{1}{2},k}|}\int_{\Gamma_{j+\frac{1}{2},k}} F(w).n \; d\Gamma = (\phi + \beta_1\phi_\eta + \beta_2\phi_{\eta\eta})_{|E} + O(h^3) \tag{2}$$

With $\phi = F.n$ and:

$$\begin{aligned} \beta_1 &= \frac{\int_\Gamma (\eta - \eta_{|E})\; d\eta}{|\Gamma_{j+\frac{1}{2},k}|} = O(h) \\ \beta_2 &= \frac{\int_\Gamma (\eta - \eta_{|E})^2\; d\eta}{2|\Gamma_{j+\frac{1}{2},k}|} = O(h^2), \end{aligned}$$

where $\eta|_E$ is the coordinate of E on the η-axis ($\eta_{|E} = 0$) and $h = |C_{j,k}C_{j+1,k}|$.
To complete the discretization of (2), we must provide third, second and first-order approximations for $\phi_{|E}$, $\phi_{\eta|E}$ and $\phi_{\eta\eta|E}$ respectively. This is done in a centered way by using weighted average and difference operators taking into account the locations of E and of the surrounding cell centers. Third-order approximation of $\phi_{|E}$ is obtained by cancelling the error term introduced by weighted average which discretizes $\phi_{|E}$ to second-order accuracy. Numerical flux is third-order accurate[13] on moderately deformed meshes and at least second-order accurate on highly distorded meshes.
If the grid deformations were neglected, the above weighted numerical flux would be reduced to:

$$F_{j+\frac{1}{2},k} = \left(\mu_1\phi - \frac{1}{8}\delta_1^2\mu_1\phi + \frac{1}{24}\delta_2^2\mu_1\phi\right)_{j+\frac{1}{2},k} \tag{3}$$

where δ_1, δ_2, μ_1 and μ_2 denote the following discrete operators:

$$
\begin{aligned}
(\delta_1 u)_{j+\frac{1}{2},k} &= u_{j+1,k} - u_{j,k}, \qquad (\delta_2 u)_{j,k+\frac{1}{2}} = u_{j,k+1} - u_{j,k} \\
(\mu_1 u)_{j+\frac{1}{2},k} &= \frac{1}{2}(u_{j+1,k} + u_{j,k}), \qquad (\mu_2 u)_{j,k+\frac{1}{2}} = \frac{1}{2}(u_{j,k+1} + u_{j,k})
\end{aligned}
$$

For 3D Euler equations, we have chosen to extend only the non-weighted numerical flux (3). As a matter of fact, this extension is heavy and difficult besides we need to determine numerous geometric parameters. More, if the mesh is regular, it is possible to preserve the third-order of accuracy with the numerical flux (3).

2.2 Volume integral

For steady problems, it is sufficient to approximate the volume integral in the unsteady term of (1) by the classical second-order formula:

$$
\frac{d}{dt}\int_{\Omega_{j,k}} w \, d\Omega = |\Omega_{j,k}| w_{t|j,k} + O(h^2)
$$

where $w_{t|j,k}$ is the time derivative of w at the cell center of $\Omega_{j,k}$ and $|\Omega_{j,k}|$ is the cell area. However, this volume integral term must be approximated to third-order accuracy in the general case. This can be achieved on a general structured mesh.[2] Nevertheless, for the sake of simplicity, we limit the presentation to the case of a regular Cartesian grid. Denoting the space steps by δx and δy -of the same order, say $O(h)$- the volume integral can be expanded as:

$$
(UT)_{j,k} = \frac{d}{dt}\int_{\Omega_{j,k}} w \, d\Omega = \delta x \delta y \left(w_t + \frac{\delta x^2}{24} w_{txx} + \frac{\delta y^2}{24} w_{tyy} \right)_{j,k} + O(h^4)
$$

Using the local form of the conservation laws:

$$
w_t = -f_x - g_y,
$$

The unsteady term becomes:

$$
\frac{1}{\delta x \delta y}(UT)_{j,k} = (w_t)_{j,k} - \frac{\delta x^2}{24}(f_{xxx} + g_{xxy})_{j,k} - \frac{\delta y^2}{24}(f_{xyy} + g_{yyy})_{j,k} + O(h^4)
$$

Using the above discrete operators δ_1, δ_2, μ_1 and μ_2, a fourth-order approximation of the unsteady term is:

$$
\frac{1}{\delta x \delta y}(\tilde{UT})_{j,k} = (w_t)_{j,k} - \frac{1}{24}\left(\frac{\delta_1^3 \mu_1 f}{\delta x} + \frac{\delta_1^2 \delta_2 \mu_2 g}{\delta y} + \frac{\delta_1 \mu_1 \delta_2^2 f}{\delta x} + \frac{\delta_2^3 \mu_2 g}{\delta y} \right)_{j,k}
$$

which can also be written as:

$$
\frac{1}{\delta x \delta y}(\tilde{UT})_{j,k} = (w_t)_{j,k} - \frac{1}{24}\left[\frac{\delta_1}{\delta x}(\delta_1^2 + \delta_2^2)\mu_1 f \right]_{j,k} - \frac{1}{24}\left[\frac{\delta_2}{\delta y}(\delta_1^2 + \delta_2^2)\mu_2 g \right]_{j,k} \tag{4}
$$

The time derivative has also to be accurately approximated.

The discretization (4) can be directly applied on curvilinear meshes, it is possible to preserve third-order accuracy of the volume integral on a regular mesh. For an unsteady problem, a classical second-order Runge-Kutta method with implicit residual smoothing[9] is used. For a steady problem, an implicit method based on the first-order backward Euler method is chosen to get a quick convergence to the steady-state and is efficiently solved using a LU relaxation algorithm[11] . The semi-discrete schemes corresponding to the weighted flux (2) and the non weighted flux (3) with a third-order approximation of volume integral are respectively called FVW3 and FV3 schemes.

2.3 Formulation of the scheme on a regular Cartesian mesh

Let us express the complete scheme for computing unsteady flows on a regular Cartesian grid, since this type of grid is our main concern in our mesh adaptation technique. Here, we combine the fourth-order accurate volume integral term (4) with the numerical flux which reduces to (3) with $\phi = f$ on $\Gamma_{j+\frac{1}{2},k}$ and $\phi = g$ on $\Gamma_{j,k+\frac{1}{2}}$, that is:

$$
\begin{aligned}
F_{j+\frac{1}{2},k} &= \left[(I - \frac{1}{8}\delta_1^2 + \frac{1}{24}\delta_2^2)\mu_1 f \right]_{j+\frac{1}{2},k} \\
F_{j,k+\frac{1}{2}} &= \left[(I - \frac{1}{8}\delta_2^2 + \frac{1}{24}\delta_1^2)\mu_2 g \right]_{j,k+\frac{1}{2}}
\end{aligned}
$$

The finite-volume scheme becomes:

$$
\frac{1}{\delta x \delta y}(UT)_{j,k} + (\frac{\delta_1 F}{\delta x})_{j,k} + (\frac{\delta_2 F}{\delta y})_{j,k} = 0
$$

and can be rewritten in the very simple form:

$$
\left[w_t + \frac{\delta_1}{\delta x}(I - \frac{1}{6}\delta_1^2)\mu_1 f + \frac{\delta_2}{\delta y}(I - \frac{1}{6}\delta_2^2)\mu_2 g \right]_{j,k} = 0 \tag{5}
$$

This Cartesian scheme is purely directional, i.e it involves points only in the x and y directions passing through the cell center $C_{j,k}$. This formulation of the third-order of numerical scheme on regular Cartesian grids, which can be seen as a finite difference formulation, is strictly equivalent to the finite volume approach. The expression (5) is much simpler than the general finite volume formula and will be implemented this way on the Cartesian grids of the mesh adaptation method for efficiency reasons. This specific formulation on Cartesian grids is called DNC.

2.4 Numerical dissipation

Centered schemes are nondissipative and are therefore subject to numerical instabilites due to the growth of high-frequency modes. Consequently, the Jameson artificial dissipation[5] is incorporated with DNC, FV3 and FVW3 formulations.

For instance for the Cartesian scheme, this leads to modify the numerical fluxes in the j direction (with similar modification in the k direction) as follows:

$$F_{j+\frac{1}{2},k} = (F - D)_{j+\frac{1}{2},k}$$

with the dissipation:

$$(D)_{j+\frac{1}{2},k} \quad = \quad \rho(\overline{A}_{j+\frac{1}{2},k})(\epsilon_2\delta_1 w - \epsilon_4\delta_1^3 w)_{j+\frac{1}{2},k}$$

where $\overline{A}_{j+\frac{1}{2},k}$ is an average of the Jacobian matrix $A = df/dw$, $\rho(A)$ denotes the spectral radius of matrix A and:

$$\epsilon_{2|j+\frac{1}{2},k} = k_2 \max(\nu_{j,k}, \nu_{j+1,k}), \quad \epsilon_{4|j+\frac{1}{2},k} = \max(0, k_4 - \epsilon_{2|j+\frac{1}{2},k})$$

$$\nu_{j,k} = \frac{|p_{j+1,k} - 2p_{j,k} + p_{j-1,k}|}{|p_{j+1,k} + 2p_{j,k} + p_{j-1,k}|}$$

where p is the static pressure and k_2, k_4 are constant parameters. In a region where w is smooth, $\epsilon_2 = O(h^2)$ and $\epsilon_4 = O(1)$, so that the dissipative terms are $O(h^3)$ and the whole scheme remains third-order accurate.

2.5 Fifth-order finite difference scheme on Cartesian meshes

A general formulation of upwind schemes of any order of accuracy has been proposed by Lerat et Corre.[8] On a regular 1-D mesh, the upwind fifth-order schemes is written in one-space dimension as:

$$(w_t)_j + \frac{\delta}{\delta x}\left(I - \frac{1}{6}\delta^2 + \frac{1}{30}\delta^4\right)(\mu f)_j = \frac{1}{60}\frac{\delta}{\delta x}\left(|A^R|\delta^5 w\right)_j$$

The left-hand side corresponds to a centered of 6^{th} order accuracy. The upwinding appears in the righ-hand side as a numerical dissipation of order $O(\delta x^5)$. Here A^R denotes the standard Roe average matrix. In the present paper, we use a simplified version of the above scheme obtained by replacing the matricial dissipation by a scalar one, i.e by replacing $|A^R|$ by the spectral radius $\rho(\bar{A})$. On a multidimensional Cartesian grid, the scheme is applied direction by direction. In the 2-D case, the scheme (called DNC5) reads:

$$\begin{aligned}(w_t)_{j,k} \quad &+ \quad \frac{\delta_1}{\delta x}\left(I - \frac{1}{6}\delta_1^2 + \frac{1}{30}\delta_1^4\right)\mu_1 f_{j,k} + \frac{\delta_2}{\delta y}\left(I - \frac{1}{6}\delta_2^2 + \frac{1}{30}\delta_2^4\right)\mu_2 g_{j,k} \\ &= \quad \frac{1}{60}\left(\frac{\delta_1}{\delta x}(\rho(\bar{A})\delta_1^5 w) + \frac{\delta_2}{\delta y}(\rho(\bar{B})\delta_2^5 w)\right)_{j,k}\end{aligned} \tag{6}$$

where $\bar{B}$ is an average of the Jacobian matrix $B = dg/dw$.
The DNC5 formulation (6) is not extended to fifth-order of accuracy on curvilinear meshes since the hypothesis of mesh regularity would be very restricting. Besides, in the mesh adaptation, vortex structures are mainly captured by Cartesian grids, a very accurate scheme is really an issue for Cartesian meshes. Temporal methods used with DNC5 formulation are similar to second-order and third-order schemes.

3 High-order mesh adaptation method

The mesh adaptation method of Meakin is based on Chimera technique and provides automatic generation and adaptation. First, the user must generate curvilinear grids aournd the bodies called “body” grids. The complete computational domain is subdivided into overlapping structured Cartesian grids, automatically generated and adapted. A refinement indicator, computed on the mesh, drives the choice of the adaptive Cartesian grid.

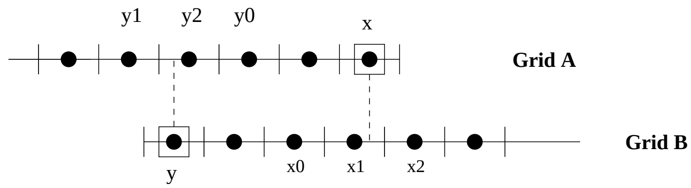

Figure 2: *Interpolated points for high-order Chimera*

The mesh adapted to the refinement indicator is generated by determining homogeneous clusters in the refinement field. For this purpose, the algorithm makes use of a dichotomic/fusion approach. Then, on each cluster an uniform Cartesian grid is generated. The user determines a multiplicator coefficient corresponding to a growing factor allowing to control the number of points after a remeshing. Because of non-coincident nature of overlap regions between grids, interpolations are necessary to allow the grids to communicate with each other. For high-order numerical schemes, Chesshire and Henshaw demonstrated that linear interpolation is not sufficient to maintain the overall global accuracy of an overset-grid technique at the same order as the interior numerical scheme. The interpolation procedure is based on directional Lagrange polynomials. For DNC and DNC5 formulations, the numerical solution on Grid A at point x is interpolated from the points x_0, x_1 and x_2 located on Grid B, the formulae usually used is:

$$w(x) = \sum_{j=0}^{2} w_j l_j(x), \quad l_j(x) = \frac{\Pi_{k=0,k\neq j}^{2}(x - x_k)}{\Pi_{k=0,k\neq j}^{2}(x_j - x_k)}$$

In order to be more accurate, the third point on Grid B x_0 is chosen such as:

$$\begin{cases} x_0 &= x_1 - \delta x \quad \text{if} \quad |x - x_1| < \dfrac{\delta x}{2} \\ x_0 &= x_2 + \delta x \quad \text{otherwise} \end{cases}$$

In the overlap region, the number of grid points has to be sufficient to ensure a proper communication between the grids. Especially, an interpolated point must be computed from interior points. If a valid interpolation cell cannot be found, the interpolated point is called an orphan point. In our technique, in order to diminish the occurance of orphan points, only one layer of interpolated cell is chosen, even for second-order centered Jameson scheme in 1D as proposed in Ref.[6] .DNC and DNC5 formulations are respectively five-point and seven-point stencil schemes and they must be of course reformulated near interpolated points in order to preserve the global order of accuracy.

3.0.1 Modification of schemes on Cartesian grids

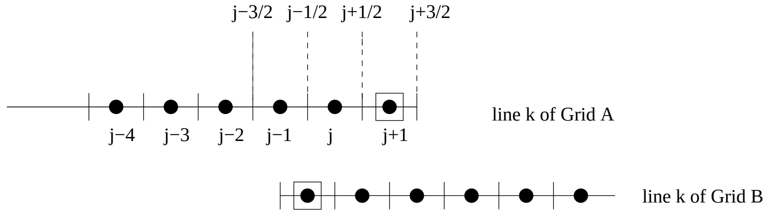

Figure 3: *Minimum overlap with one layer of interpolated cells*

In figure 3, the values on the last cell face $(j+\frac{3}{2},k)$ of Grid A are always interpolable by Lagrange interpolation, otherwise Grid B would be too small and thus useless. For DNC formulation, the current formula can be used until the face $(j-\frac{1}{2},k)$. On the other hand, a specific treatment based on upwind formulae is performed for the calculation of physical flux and the artificial viscosity flux at the face $(j+\frac{1}{2},k)$:

$$
\begin{aligned}
F_{j+\frac{1}{2},k} &= -\frac{1}{84}f_{j-2,k} - \frac{1}{60}f_{j-1,k} + \frac{5}{12}f_{j,k} + \frac{11}{12}f_{j+1,k} - \frac{32}{105}f_{j+\frac{3}{2},k} \\
F_{j-\frac{1}{2},k} &= -\frac{1}{12}f_{j-2,k} + \frac{7}{12}f_{j-1,k} + \frac{7}{12}f_{j,k} - \frac{1}{12}f_{j+1,k} \\
D_{j+\frac{1}{2},k} &= \rho(\bar{A})_{j+\frac{1}{2},k}\left(\epsilon_2(w_{j+1,k}-w_{j,k}) - \epsilon_4(-w_{j-1,k} + \frac{10}{3}w_{j,k} - 5w_{j+1,k} + \frac{8}{3}w_{j+\frac{3}{2},k})\right) \\
D_{j-\frac{1}{2},k} &= \rho(\bar{A})_{j-\frac{1}{2},k}\left(\epsilon_2(w_{j,k}-w_{j-1,k}) - \epsilon_4(-w_{j-2,k} + 3w_{j-1,k} - 3w_{j,k} + w_{j+1,k})\right)
\end{aligned}
$$

with :

$$
\nu_{j+1,k} = \frac{|2p_{j,k} + \frac{16}{5}p_{j+\frac{3}{2},k} - \frac{1}{5}p_{j-1,k} - 5p_{j+1,k}|}{|2p_{j,k} + \frac{16}{5}p_{j+\frac{3}{2},k} + \frac{1}{5}p_{j-1,k} + 5p_{j+1,k}|}
$$

These formulae allow to preserve the global third-order of accuracy of the overset method. The DNC5 formulation can be applied until the face $(j-\frac{3}{2},k)$. We construct sixth-order upwind formulae in order to evaluate physical flux at face $(j-\frac{1}{2},k)$ and $(j+\frac{1}{2},k)$.

$$
\begin{aligned}
F_{j-\frac{3}{2},k} &= \frac{1}{60}f_{j-4,k} - \frac{2}{15}f_{j-3,k} + \frac{37}{60}f_{j-2,k} + \frac{37}{60}f_{j-1,k} - \frac{2}{15}f_{j,k} + \frac{1}{60}f_{j+1,k} \\
F_{j-\frac{1}{2},k} &= \frac{1}{660}f_{j-4,k} + \frac{1}{180}f_{j-3,k} - \frac{41}{420}f_{j-2,k} + \frac{11}{20}f_{j-1,k} + \frac{7}{10}f_{j,k} - \frac{7}{30}f_{j+1,k} + \frac{256}{3465}f_{j+\frac{3}{2},k} \\
F_{j+\frac{1}{2},k} &= \frac{1}{66}f_{j-4,k} - \frac{19}{180}f_{j-3,k} + \frac{139}{420}f_{j-2,k} - \frac{13}{20}f_{j-1,k} + \frac{67}{60}f_{j,k} + \frac{11}{30}f_{j+1,k} - \frac{256}{3465}f_{j+\frac{3}{2},k}
\end{aligned}
$$

For numerical dissipation, a fifth-order formula is retained in order to determine the values at the face $(j-\frac{1}{2},k)$ but for stability reasons, only a third-order formula is chosen at the face $(j+\frac{1}{2},k)$:

$$
\begin{aligned}
D_{j-\frac{3}{2},k} &= \frac{1}{60}\rho(\bar{A})_{j-\frac{3}{2},k}\left(-w_{j-4,k} + 5w_{j-3,k} + 10w_{j-2,k} + 10w_{j-1,k} + 5w_{j,k} + w_{j+1,k}\right) \\
D_{j-\frac{1}{2},k} &= \frac{1}{60}\rho(\bar{A})_{j-\frac{1}{2},k}(\frac{1}{11}w_{j-4,k} - \frac{5}{3}w_{j-3,k} + \frac{50}{7}w_{j-2,k} - 14w_{j-1,k} + 15w_{j,k} - 11w_{j+1,k} \\
&- 11w_{j+1,k} + \frac{1024}{231}w_{j+\frac{3}{2},k}) \\
D_{j+\frac{1}{2},k} &= \frac{1}{60}\rho(\bar{A})_{j+\frac{1}{2},k}(\frac{6}{5}w_{j-1,k} + 4w_j - 6w_{j+1,k} + \frac{16}{5}w_{j+\frac{3}{2},k})
\end{aligned}
$$

3.0.2 Modification of schemes on curvilinear grids

For a regular curvilinear mesh, the discretizations of numerical flux (3) and volume integral (4) can be third-order accurate, the treatment in overlap region is consequently based on non-weighted formula. We use the formulation FVW3 until the face $(j+\frac{1}{2},k)$. At the face $(j+\frac{1}{2},k)$, an upwind formula is applied to preserve third-order accuracy of the physical flux and volume integral corresponding to FV3 formulation:

$$
\begin{aligned}
F_{j+\frac{1}{2},k} &= -\frac{1}{16}\phi_{j-1,k} + \frac{13}{24}\phi_{j,k} + \frac{11}{16}\phi_{j+1,k} - \frac{1}{6}\phi_{j+\frac{3}{2},k} + \frac{1}{24}\delta_2^2\mu_1\phi_{j+\frac{1}{2},k} \\
(UT)_{j+\frac{1}{2},k} &= -\frac{1}{48}f_{j-1,k} - \frac{5}{144}f_{j,k} - \frac{1}{144}f_{j+1,k} + \frac{1}{16}f_{j+\frac{3}{2},k} - \frac{1}{24}\delta_2^2\mu_1 f_{j+\frac{1}{2},k}
\end{aligned}
$$

4 Numerical results

4.1 Numerical simulation of 2D parallel blade-vortex interaction

The first test case is the numerical simulation of a 2D blade vortex interaction and is chosen to be both realistic and comparable with an experiment carried out by Caradonna et al in.[7]

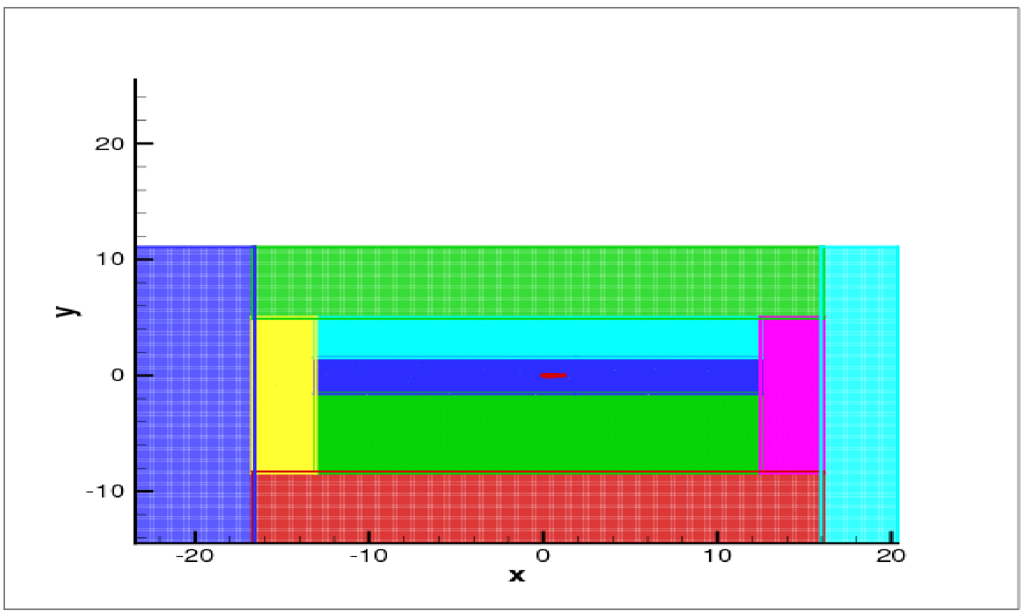

Figure 4: *View of global mesh*

The vortex is located approximatively 0.25 chord below the profile and clockwise-rotating. It is created using the Scully algebraic model which represents the best core model according to the experiment. With this model, the tangential velocity equation in the vortex frame in dimensionless form is expressed by:

$$v_\theta = \frac{\Gamma_v}{2\Pi}\frac{r}{r^2+\xi_v^2}$$

where the vortex circulation is $\Gamma_v = 0.2536$ and the core radius is $\xi_v = 0.162$. The vortex is located at $(x_0, y_0) = (-10; -0.25)$. The goal of this section is to compare the perservation of vortex during the advection phasis with second-order, third-order and fifth-order methods. The global mesh consists of a body grid around a NACA0012 airfoil and 9 Cartesian blocks with overlap. The reference mesh on Figure 4 is made of 230000 cells, the finest space step is equal to $h = 0.05$ and the radius core is discretized by 6 points. A second mesh containing 460000 cells is used for the computations. For the second-order method, the classical second-order centered Jameson scheme is employed. For third-order and fifth-order methods, we use respectively DNC and DNC5 formulations on Cartesian grids and FVW3 formulation on curvilinear grid. The comparison of the pressure coefficient distribution at two different airfoil sections performed with second-order, FVW3/DNC and FVW3/DNC5 methods are shown on Figures 5 and 6. On the coarse mesh, the Cp values obtained with second-order method are slightly more important than NASA experiment when the vortex reaches the body. With third-order and five-order methods, the peak of Cp values at $t = 0$ is correctly predicted. On the fine mesh, the Cp curves are very similar apart from the method applied.

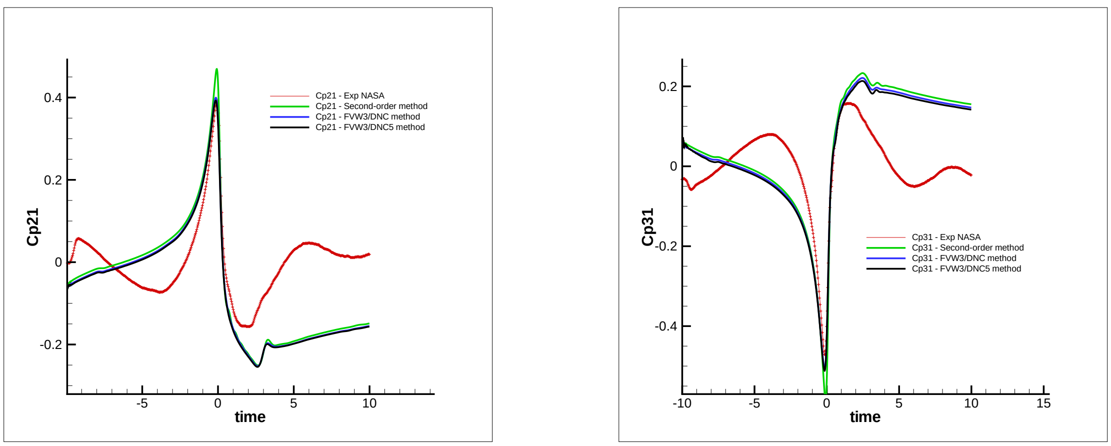

Figure 5: *Coefficient pressure on the coarse mesh*

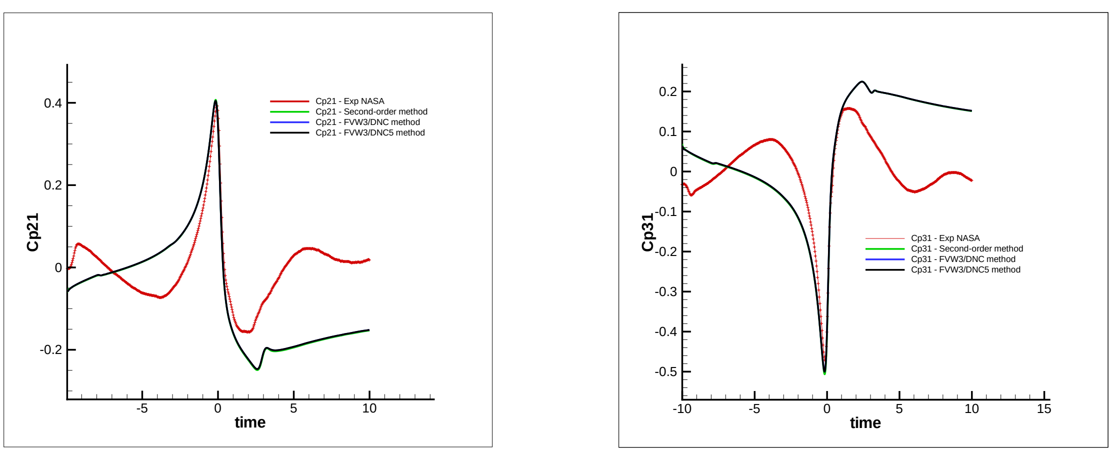

Figure 6: *Coefficient pressure on the fine mesh*

The vorticity is extracted between $t = -10$ and $t = -1$ from a horizontal line passing through the vortex center until it reaches the airfoil reaches the airfoil. Figure 7 illustrates the vorticity loss in the vortex core for the coarse and the fine meshes during the advection phasis with second-order, FVW3/DNC and FVW3/DNC5 methods. On the coarse mesh, oscillations appear to the level of the peak with second-order method and numerical diffusion is significant, the vorticity losses are 36%. The use of high-order schemes allows to reduce vorticity losses since it is found to be 24% with FVW3/DNC method and only 12% with five-order formulation on Cartesian grids. Besides, dispersive error of centered Jameson scheme have an armful effect on the vortex location which deviates from its initial position during the advection phasis. On the other hand, it is well-located when applying high-order methods. On the fine mesh, the radius core is discretized by 13 points, it allows to reduce dispersive and dissipative errors, since the loss rate is around 10% for second and third order computations and only 1.7% with FVW3/DNC5 method.

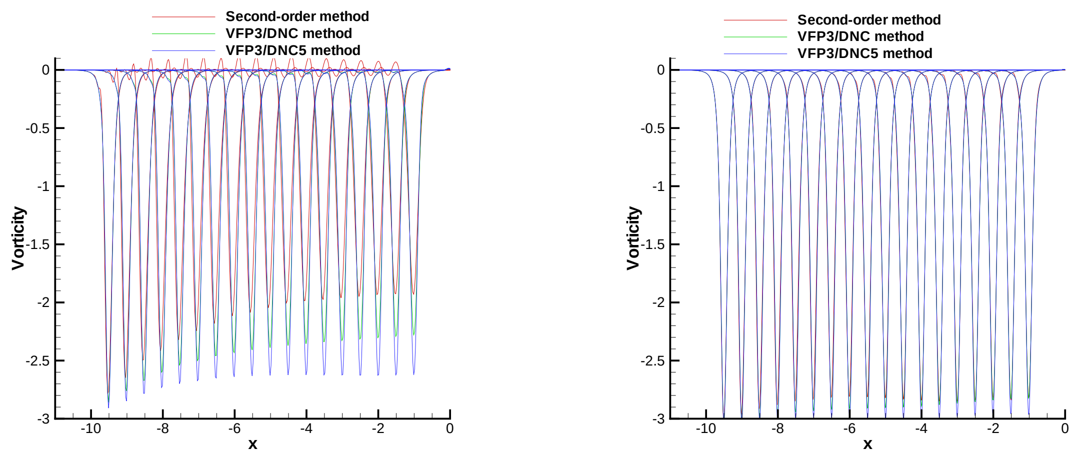

Figure 7: *Vorticity loss during the advection phasis on the coarse and the fine meshes*

4.2 Inviscid flow around a helicopter blade

In this section, the high-order methods are applied to the computation of an isolated blade of ONERA 7A helicopter rotor in hover solving the Euler equations. Automatic generation and adaptation procedures are used. The flight conditions are given by a tip Mach number of $M_{tip} = 0.662$ and a collective pitch angle of $\Theta_c = 7.5\,°$. The aim of this section is to capture accurately the tip vortex emitted at the blade tip and to measure the improvements by comparing the results obtained with second-order method. The blade mesh is made of $140 \times 26 \times 17$ cells. From this blade mesh, three background Cartesian meshes are automatically generated. The procedure generates 8 overlapping Cartesian blocks for each backround mesh with respectively 140000, 280000 and 560000 points. The finest space steps are respectively equals to $h = 0.136$, $h = 0.068$ and $h = 0.034$ on the coarse, medium and fine mesh. For the three calculations, the mesh is adapted to the numerical solution and the refinement indicator is the rotational of velocity. The Cartesian grid are adapted every 800 iterations and 10 remeshings are performed.

The user controlles the total number of points by a growing factor chosen equal to 1.4 in this study. After the last remeshing, the number of points is respectively around equal to 4.5 millions on the coarse mesh, 11 millions on the medium mesh and 44 millions on the fine mesh. The adapted medium mesh and iso-vorticity surfaces are displayed on Figure

Figure 8: *View of the blade*

9. On this mesh, the finest space step is equal to $h = 3.75.10^{-3}$, it corresponds to 2 cells in the vortex core radius. We observe that the background mesh is refined in the vortex path. The results obtained show that differences between second-order and FV3/DNC methods are not significant, the third-order method allows to follow the vortex on a lightly more important age, around 180 degrees of age. The improvements obtained with the FV3/DNC5 method are on the other hand considerable: it is possible to follow the vortex for approximatively one revolution. The evolution of maximum of vorticity as a function of vortex age is represented on Figure 10 on coarse, medium and fine mesh. On the coarse mesh, the maximum of vorticity is equal to 10 with all the methods. During the first 40 degrees of age, the vorticity decreases abruptly, the losses are nearly 40%, this phenomenon seems to be independent of the numerical diffusion and the mesh resolution since it appears also on the medium and the fine meshes. On the other hand, after 30 degres of age, the vorticity goes on reducing regularly, this is due to the low density of the mesh and to an important diffusion of numerical schemes. Nethertheless, the FV3/DNC5 method enables to limit these losses on vorticity in comparison with second-order and third-order methods. On the fine mesh, the maximum vorticity at the blade tip is 4 times higher than the one obtained on the coarse mesh. The FV3/DNC5 method is really more accurate since it is possible to preserve big values of the vorticity, higher than 15, on 360 degrees of age. Finally, the fifth-order method enables to solve this problem with comparable computational cost to classical method.

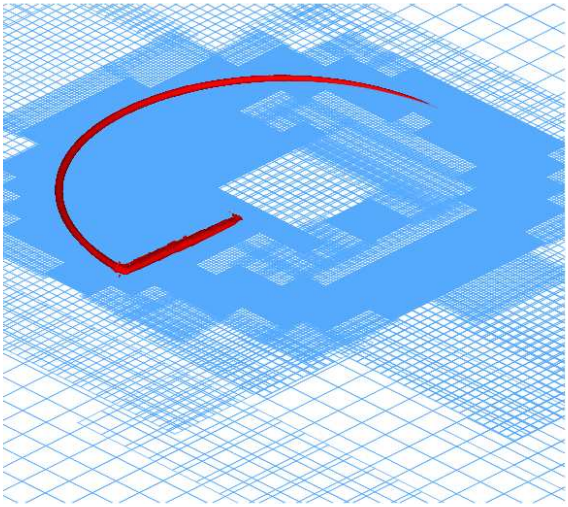

Second-order method

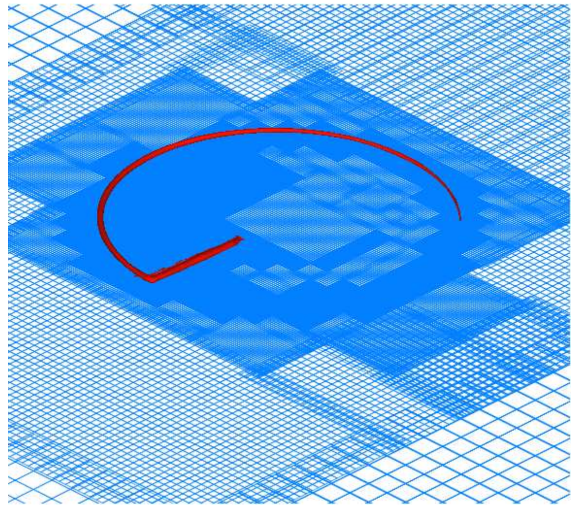

FV3/DNC method

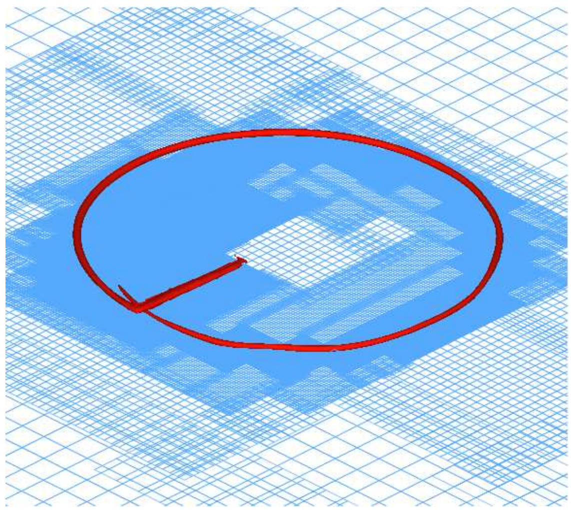

FV3/DNC5 method

Figure 9: *Vorticity iso-surface ($||\vec{rot}\ \vec{V}|| = 5$) on the medium mesh*

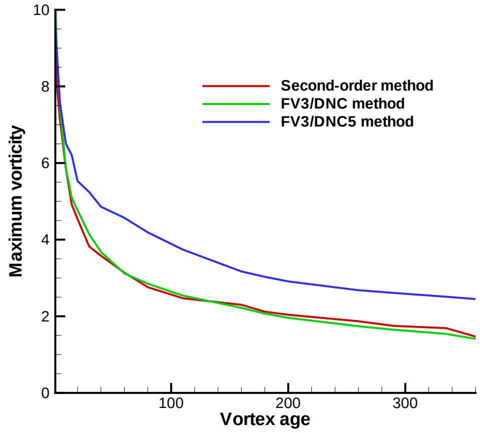

Coarse mesh

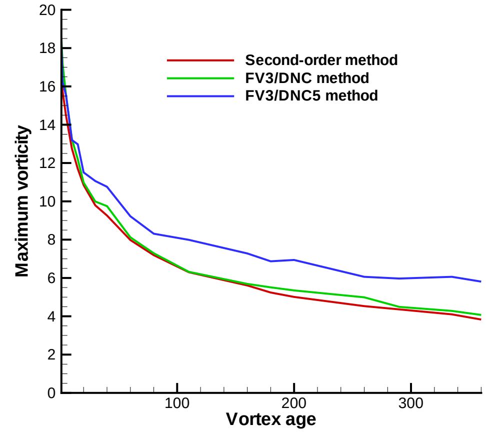

Medium mesh

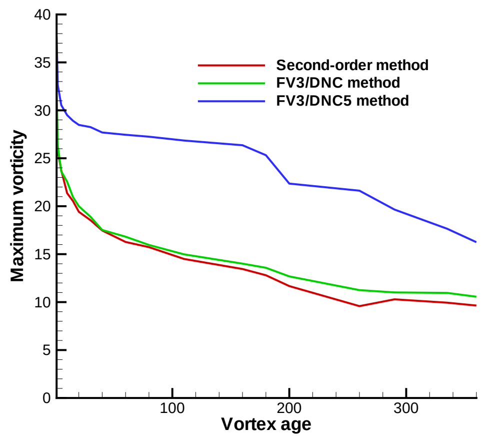

Fine mesh

Figure 10: *Maximum vorticity in the vortex core*

5 Conclusion

In this paper, we have presented a high-order mesh adaptation method for the compressible Euler equations. The procedure generates automatically uniform structured Cartesian grids whereas the user provides a short and fine curvilinear grid around the bodies. On curvilinear meshes, the numerical scheme is based on a third-order finite volume method whereas third-order and fifth-order explicit centered finite difference formulations are constructed on Cartesian grids. In overlap regions, numerical solution is obtained by high-order interpolation by using Chimera technique. In addition, high-order boundary formulations are suggested in order to reduce the overlap constraints and to maintain the same order of accuracy on all the domain. The simulation of blade-vortex interaction demonstrates the ability of fifth-order scheme to preserve the vortex during the advection phasis. Application of the high-order method to compute an inviscid flow around a hovering blade of the ONERA 7A helicopter rotor confirms that fifth-order scheme on Cartesian grids combined with a grid with 4 cells in the radius core of the vortex allows to capture the tip vortex over large distances.

References

[1] C. Benoit and G. Jeanfaivre, *Three dimensional inviscid isolated rotor calculations using chimera and automatic Cartesian partitioning methods*, Journal of the American Helicopter Society, (2003), pp. 128–138.

[2] P. Cinnella, *Simulation d'écoulements compressibles turbulents autour de profils oscillants par une méthode numérique de haute precision*, PhD thesis, Ecole Nationale Superieure d'Arts et Metiers, Paris, 1999.

[3] P. Cinnella and A. Lerat, *A study of turbulent compressible flows over oscillating airfoils using a high-order numerical scheme*, Computational Fluid Dynamics Journal special issue, 9 (2001), pp. 257–271.

[4] N. Hariharan and L. Sankar, *High-order numerical simulations of rotor flow field*, in 50^{th} Annual Helicopter Society Forum, vol. 2, Washington DC, 1992.

[5] A. Jameson, W. Schmidt, and E. Turkel, *Numerical solutions of the Euler equations by finite volume methods using Runge-Kutta time stepping*, AIAA Paper, 81-1259 (1981).

[6] G. Jeanfaivre, C. Benoit, and M. L. Pape, *Improvement of the robustness of the chimera method*, in 32^{nd} AIAA Fluid Dynamics Conference, AIAA paper 2002-3290, June 2002.

[7] C. Kitaplioglu, F. X. Caradonna, and M. McCluer, *An Experimental Study of Parallel Blade-Vortex Interaction Aerodynamics and Acoustics Utilizing an Independtly Generated Vortex*, NASA/TM-1999-208790, 1999.

[8] A. Lerat and C. Corre, *High-Order residual-based compact schemes on structured grids*, Higher Discretization Methods VKI LS 2006-01, 2006.

[9] A. Lerat, J. Sides, and V. Daru, *An implicit finite-volume method for solving Euler equations*, Lecture Notes in Physics, 170 (1982), pp. 343–349.

[10] R. Meakin, *An Efficient Means of Adaptive Refinement Within Systems of Overset Grids*, in 12^{th} AIAA Fluid Dynamics Conference, AIAA paper 95-1722-CP, 1995.

[11] J. Peter and F. Drullion, *Large stencil viscous flux linearization for the simulation of 3D compressible turbulent flows with backward-Euler schemes*, Computers and Fluids, 36 (2007), pp. 1005–1027.

[12] M. Rai, *Navier-stokes simulations of blade-vortex interaction using high-order accurate upwind schemes*, AIAA Paper, (1987).

[13] A. Rezgui, P. Cinnella, and A. Lerat, *Third-order accurate finite volume schemes for Euler computations on curvilinear meshes*, Computers and Fluids, 30 (2001), pp. 875–901.

[14] R. Strawn and J. Ahmad, *Computational modeling of hovering rotors and wakes*, AIAA Paper, (2000).

[15] R. Strawn and T. Barth, *A finite-volume euler solver for computing rotary-wing aerodynamics of unstructured meshes*, in 48^{th} annual helicopter society forum, vol. 1, 1992.

[16] B. Wake and D. Choi, *Investigation of high-order upwinded differencing for vortex convection*, AIAA Journal, 34 (1996), pp. 332–337.